A Comparative Study of MPPTs for Nano-Satellite Microgrid Applications under Spinning Flight Scenarios

Yaqoob, Mohammad; Abubakr, Hussein; Alcala, Jose Matas; Lashab, Abderezak; Guerrero, Josep M.; Vasquez, Juan C.

Published in:
IECON 2022 – 48th Annual Conference of the IEEE Industrial Electronics Society

DOI (link to publication from Publisher):
10.1109/IECON49645.2022.9968896

Publication date:
2022

Document Version
Accepted author manuscript, peer reviewed version

A Comparative Study of MPPTs for Nano-Satellite Microgrid Applications under Spinning Flight Scenarios

Mohammad Yaqoob[1*], Hussein Abubakr[1], Jose Matas Alcala[2], Abderezak Lashab[1], Josep M. Guerrero[1], Juan C. Vasquez[1]
[1]*Center for Research on Microgrids (CROM), AAU Energy, Aalborg University, 9220 Aalborg, Denmark.*
[*] *Electrical Engineering Department, Balochistan UET Khuzdar, Khuzdar 89100, Pakistan.*
[2]*Electric Engineering Department, Polytechnic University of Catalonia (EEBE-UPC), 08019 Barcelona, Spain.*
Corresponding Author Email: mya@energy.aau.dk

***Abstract*—This paper offers a comparative analysis of Maximum Power Point Tracking (MPPTs) techniques under the spinning conditions for small satellite applications. The Nano Satellite (NanoSat) is constrained on volume and mass with body-mounted solar panels and where it is dedicated to some special orientation scenarios, depending on specific mission requirements. This results in irregular solar irradiance on the PV system; thus, it needs an efficient and effective strategy to extract the maximum power transferred to the loads in the NanoSat Electrical Power System (EPS). While the EPS can be regarded a space microgrid due to control and coordination in a small electric network of distributed generations (DGs), storage, and loads. Therefore, some well-known MPPT techniques are investigated where different scenarios are carried out among conventional Perturb and Observe (P&O), Incremental Conductance (IC), and Ripple Correlation Control (RCC) to highlight the optimal MPPT extractions for NanoSat applications. The system was developed and modeled in MATLAB/SIMULINK and the final findings demonstrate that the RCC provides smooth power compared to other ones, while the other ones offer an oscillated power under the effect of radiations change and spinning conditions for the system under test.**

Keywords—Boost Converter, Incremental Conductance, Maximum Power Point Tracking, Nano Satellite, Perturb and Observe, Ripple Correlation Control system.

I. INTRODUCTION

In recent years, small satellites of 1-10 kg standard Nano Satellites (NanoSat) have gained an enormous concentration from the diverse community of educational institutions, government organizations, and private companies; but not only limited to that. In this class, the Cube Satellite (CubeSat) is in speedy growth with dimensions of 10×10×10 cm and a mass of 1.33 kg known as 1 unit (1U). The CubeSat is extendable to further bigger units of 2U, 3U, and so on. These satellites provide solutions from space exploration to earth observation and other scientific and technological demonstrations mostly installed in Low Earth Orbit (LEO). These Nano Satellites (NanoSats) are comprised of some subsystems i.e., Attitude Determination and Control System (ADCS), Communication Transceiver (COM), Onboard Data Handling (OBDH) subsystem, Electrical Power System (EPS), and Payloads. The EPS powers the entire subsystems of the satellite for successful operations. In terms of power systems, EPS is a perfect example of a space microgrid comprising mainly Distributed Generations (DGs), a controlled coordination system, an integrated energy storage system, and loads [1], [2]. A typical SmallSat microgrid is shown in Fig. 1. However, the NanoSat microgrid is

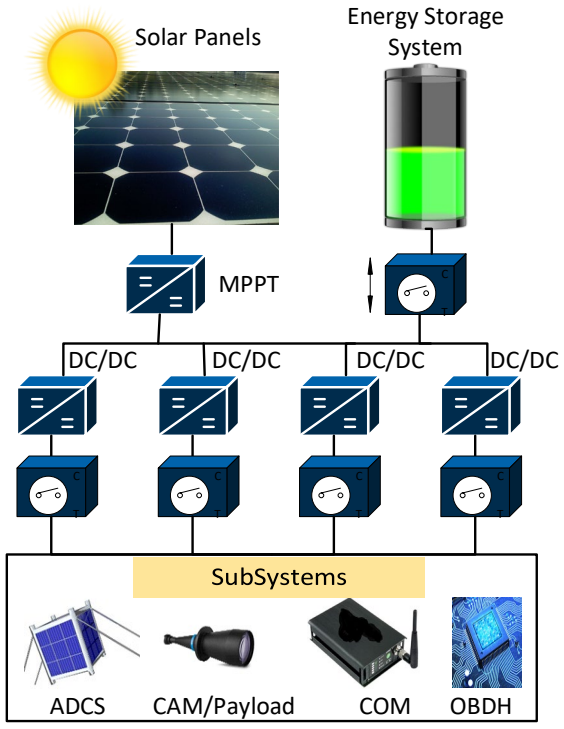

Fig. 1. A typical NanoSat microgrid.

constrained by some regulation of mass and volume while the power is generated from the body-mounted solar panels. Each LEO NanoSat follows a dedicated orbit and an orientation as per the mission requirements. From some famous orientations, i.e., Sun-pointing, nadir-pointing, and free-orientation scenarios [3]. The solar flux significantly varies in each orientation on the faces of the satellite resulting in a continues change in Nanosat's angle toward the Sun [4]. Therefore, the solar array at the Maximum Power Point Tracking (MPPT) seems to be the most suitable solution for these operation conditions, instead of the Direct Energy Transfer (DET) option [5] [6].

Recently, several maximum power point tracking techniques (MPPT) have been verified for small satellites, deep-space probes, experiment platforms for satellites, etc. [7]. Specifically, for LEO SmallSats, P&O technique is widely applied due to its ease of implementation, tracking accuracy, and low complexity. However, it suffers from several drawbacks like oscillation near the maximum power. Therefore, for space applications, we examine other essential techniques such as Incremental Conductance (IC), and Ripple Correlation Control (RCC) [8].

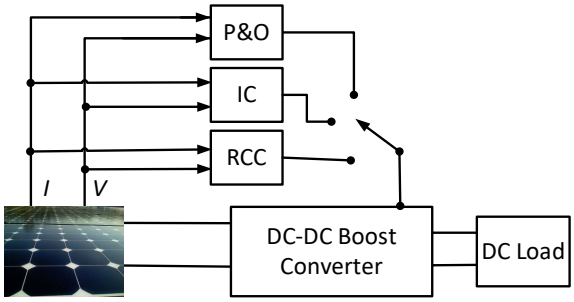

Fig. 2 Schematic diagram of the system under test.

From the above literature review, this work proposes a comparative study of the conventional P&O, IC, and RCC in two different scenarios. In the first scenario, the effect of abrupt shifts of irradiance and temperature are examined in a transient state. In the second scenario, the Sun-pointing orientation for a 3U nano CubeSat with the spin of 4rpm in standard irradiance of 1367 W/m^2 is carried out.

The rest of the paper arrangement is as follows: Section II describes the main system and the important parameters for satellite EPS operation. In sections III, and IV photovoltaic (PV) system modeling and MPPT converter operation methods are discussed, respectively. In section V, the above-discussed MPPT techniques are described. The results are shown and discussed in section VI. Furthermore, the entire paper is concluded in section VII.

II. Description of the System and Important Parameters

The system is comprised of some main parts like (a) Energy generation (b) DC-DC boost converter (c) Three MPPT techniques i.e., IC, RCC, P&O, and (d) DC resistive load as shown in the proposed schematic diagram in Fig. 2.

A. Orbital Considerations

The considered orbit is at an altitude of 700 km, Keplerian polar Sun-synchronous orbit, the most suitable low earth orbit for NanoSat which has a constant illumination of 1367 W/m^2.

B. PV Architecture

The NanoSat EPS architecture houses four solar panels on its X and Y axis, each one is composed of 6-GaAs SISP triple junction (3-J) solar cells with an efficiency of 32% at AM0, 1Sun, when subjected to 1367W/m^2, and an average temperature of 28°C. The specifications of the solar panels are given in Table I.

C. Orientation of the Satellite

The considered satellite orientation is Sun-pointing orientation, as shown in Fig. 3, to analyze the incident angle change in time behavior of the solar radiation received on the different faces of the satellite. This orientation is more efficient than the other famous orientations [16]. Where, one 3U face labeled as X- in the Figure is receiving Sunlight with maximum radiation. To achieve the mission requirements and to avoid the PV cells damage from the constant irradiance and temperature the space-craft spins axis with a rotation of 4-rpm during the orbit period. The harvested energy from the Sun irradiation by the PV panels mounted on the X and Y-axis of the NanoSat during a single spin is given in Fig. 4.

III. Photovoltaic System Modeling

The PV system is a conversion procedure of direct Sun light into electricity by applying a semiconductor *p-n* junction diode. The phenomenon is described as solar radiation

TABLE I. Specifications of 3-U CubeSat PV Panel

Name	Specifications
PV panel	Serries connected 6 SISP 32% solar cells
	*Voc = 16002 [mV], Isc = 19.0 [mA]
	*VPmax = 14100 [mV], IPmax = 18.4 [mA]

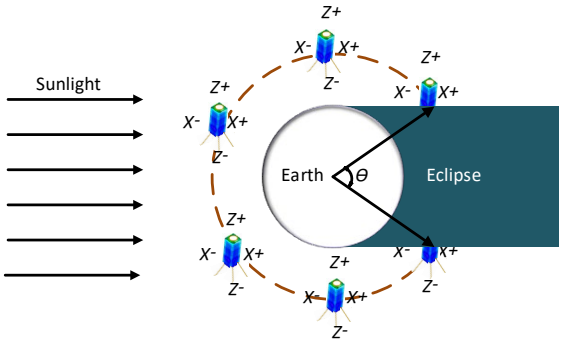

Fig. 3. The Sun-pointing orientation scenario for the case study.

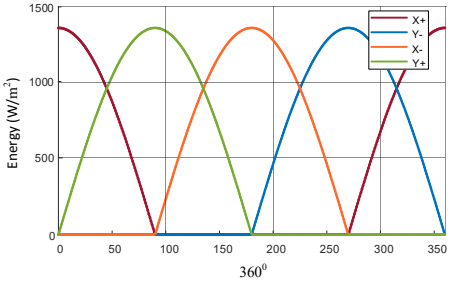

Fig. 4. The harvested energy in one spin from the X and Y sides.

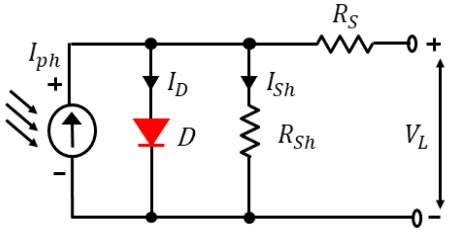

Fig. 5. Single Diode Model of Practical PV.

absorption, and transportation of carriers at *p-n* junction which results the flow of current at PV terminals [9]. The 3-J solar cells are modeled as three sub single diode model cells where each sub-cell is representing a single independent solar cell. The three equivalent solar cells are arranged in a way that enables them to be shrinking the gaps between the cells and be connected in series from top to bottom. The electrical performance (I-V diagram) of 3-J solar cells can be derived from the three sub-cells and the sum of the total cells. Each sub-cell possesses the same current because all sub-cells are connected in series. The solar panels and arrays are the combination of the cells in series-parallel configurations for the desired output voltage and current [10]. The I-V curve of a PV cell, array, or module as a continuous function for a given set of operating conditions is defined by the equivalent circuit known as the single diode model which is represented in Fig. 5. The characteristics of a single diode equation for a module or array are described by the equations:

$$I = I_{ph} - Io\left[exp\left(\frac{q(V_m + I_m R_s)}{akTN_s}\right)\right] \quad (1)$$

$$I_o = \frac{I_{sc} + K_1\,(T - T_n)}{exp\left(\frac{(V_{oc} + K_2(T - Tn))q}{akTN_s}\right)} \quad (2)$$

$$I_o = \left((T - T_n)K_1 + I_a\right)\frac{G}{G_n} \quad (3)$$

Where I_{ph} is the solar radiation generated current, Io is the reverse saturation current, V_m and I_m are the output voltage and output current of the array respectively, T is the temperature in Kelvin and G is the Sun radiation in W/m^2.

IV. MPPT CONVERTER

The DC-DC converters are power electronic circuits comprised of capacitors and inductors and semiconductor devices, through which the applied input voltage level is converted into another one at the output of the converter. The boost converter is placed at the back end for performing the MPPT as a power electronic interface. Therefore, the input voltage is enhanced corresponding to the duty ratio offered by the controller. The boost converter and control system can be seen in the circuit of the dc/dc boost converter in Fig. 6. Since in the ideal conditions, the capacitor, inductor, diode, and switch do not consume energy, therefore, two fundamental conservation laws exist between the input and the output. The first energy balance law reveals that the input energy may be equal to the output energy. The second law of charge balance stands on the input charge equal to the output charge. Because the input current can only provide charge to the output side when the switch is open, during (1-d) T in one T-period. The equations are given in (4) and (5), respectively, for the first and second law.

$$P_{in} = P_{out} \rightarrow I_{in}V_{in} = I_{out}V_{out} \quad (4)$$

$$Q_{in} = Q_{out} \rightarrow I_{in}(1-d)T = I_{out} \quad (5)$$

The basic relationship can be calculated between the input and output voltage using Eq. (4) and (5).

$$V_{out} = \frac{V_{in}}{1-d} \quad (6)$$

Where the duty cycle d is a positive number less than 1. According to this relationship, it is seen that $V_{out} > V_{in}$.

V. APPLIED MAXIMUM POWER POINT TRACKING TECHNIQUES

The main target of using MPPT approaches is to extract and track the maximum power from the solar cell under a particular radiation level by regulating the specific system voltage. Therefore, in this section short notes about P&O, IC, and RCC techniques are given.

A. Perturb and Observe Technique

This technique is the most common in practice due to its simplicity, ease of application, and low-cost implementation with a good performance. However, at the rapidly changing environmental time intervals the P&O algorithm get confused [11]. In this approach, the resulting PV current or voltage are periodically perturbed to observe their impact on the PV characteristics to attain maximum power. The system's operating point is shifted toward the MPP either by increasing (+ve) or decreasing (-ve) the current or voltage of the PV array. The power variation is determined concerning the change in voltage and the next step of perturbation is calculated and the process is repeated until the peak value is achieved when there is no difference in power, but this does not occur generally. The main procedures for the P&O

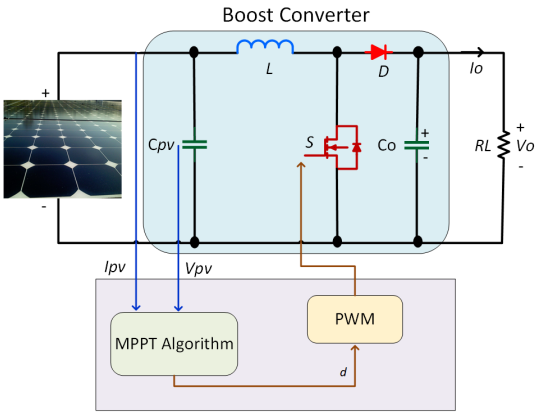

Fig. 6. Global system scheme for MPPT.

TABLE II. TRUTH TABLE FOR P&O MPPT METHOD [11]

Perturbation (ΔV)	Power change (ΔP)	Next perturbation
+	+	+D
+	-	-D
-	+	-D
-	-	+D

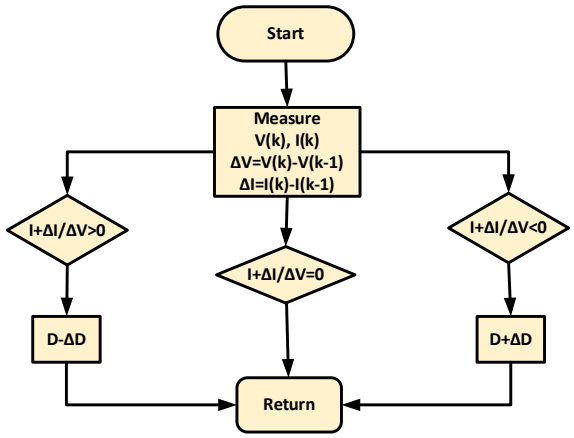

Fig. 7. Flowchart of incremental conductance algorithm.

algorithm are presented in detail in [12]. If the ΔV>0 leads to ΔP>0 then the direction of the next step is in the same direction otherwise it is in the opposite as, stated in Table II [12].

B. Incremental Conductance Control

This method is widely applied in PV power generation systems due to its high efficiency of tracking and accuracy. The overall concept of this technique is described in the flow chart shown in Fig. 7.

The IC algorithm uses the derivative P~V characteristics (conductance) of the PV array. The terminal voltage of the considered PV system is calculated relying on the instantaneous and incremental conductance [13].

$$P = VI$$

By applying the chain rule of derivatives of products,

$$\frac{\partial P}{\partial V} = \frac{[\partial(VI)]}{\partial V} = I \times \frac{\partial V}{\partial V} + V \times \frac{\partial I}{\partial V} = I + V\frac{\partial I}{\partial V} \quad (7)$$

And it can be as:

$$\frac{\partial P}{\partial I} = \frac{[\partial(VI)]}{\partial V} = I \times \frac{\partial V}{\partial I} + V \times \frac{\partial I}{\partial I} = V + I\frac{\partial V}{\partial I} \quad (8)$$

When reaching the MPP, this means that the $\frac{\partial P}{\partial V} = 0$

The MPPT controls the PWM signal of the boost converter until $\partial(I)/\partial(V) + (I/V) = 0$ is satisfied from Eq. 7. The module's max power set as > 98% of its incremental conductance. There are three basic conditions for $\frac{\partial P}{\partial V}$, which must be taken into consideration: First, when $\frac{\partial P}{\partial V} > 0$, means that the panel is running on the left side of the MPP, so some changes are required to be made to the right. Second, when $\frac{\partial P}{\partial V} < 0$, means that the operating point lies on the right side of the MPP, so some changes ought to be made to the left. Last, when the change $\frac{\partial P}{\partial V} = 0$, in this case, the solar panel is working exactly at the MPP, so no need to make any change [14].

C. Ripple Correlation Control

This method is based on the input current of the boost converter which comprises a DC component I_L and a ripple component. The I_L is set regarding the level of temperature and amount of radiation. Thus, the output power is a mixture of ripple and mean components that vary nonlinearly with I_L as described in Fig. 8 [15]. The objective is to force I_L to track $I_L{}^*$corresponding to the MPP regardless of irradiance, temperature, or other variances [16]. The RCC block diagram is shown in Fig. 9.

The idea here is to correlate the inductor's current I_L towards i_L* to achieve the MPP so we must define whether I_L is low/high than I_L*. If $I_L < I_L{}^*$, it means that the ripple for current and power are in phase so the $\frac{dp}{dt} \times \frac{di_L}{dt}$ is positive (>0). Also, if the $I_L < I_L{}^*$, it means that $\frac{dp}{dt} \times \frac{di_L}{dt}$ is negative (< 0). A high pass filter is used in this technique to separate the DC component. The time derivatives of the current and power are not equal to zero due to the inherent ripples found by the switching process of the converter and can be deduced as follows [16]:

$$d = k.\int \frac{dp}{dt} \times \frac{di_L}{sdt}\, dt \qquad (9)$$

where d is the duty cycle and k is the constant (+ve gain). The inductor current decreases and increases depending on the duty cycle d, whereby adjusting d appropriate IL is achieved.

VI. RESULTS AND DISCUSSION

A. PV Array Characteristics

The nonlinear behavior of the I-V and P-V characteristics is obtained according to varying irradiance and temperature for the 3U CubeSat designed PV panel discussed in Table I. The open-circuit voltage, short circuit current, and change in maximum power can be observed in Fig. 10 (a) and (b). When the operating temperature increases, the change in the short circuit current is negligible as can be seen in Fig. 10 (a). However, an increase in the operating temperature leads to a decrease in the open-circuit voltage of the PV, similarly, the maximum power reduces. While a decrease in the operating temperature results in an increase in maximum power and a negligible change in short circuit current.

On increasing the photonic radiation level, the change in open circuit voltage is negligible, which is reflected in Fig. 10 (b). However, the increase in the irradiation level leads to an increase in the maximum current and equally the maximum power of the PV. While a decrease in the irradiance level

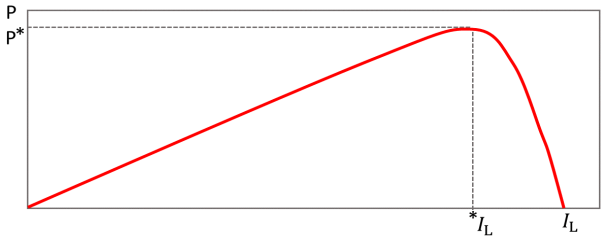

Fig. 8. PV array average current and power [11].

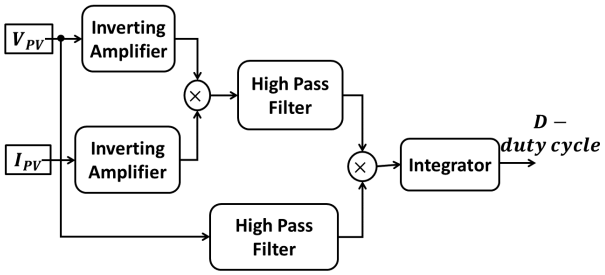

Fig. 9. RCC block diagram.

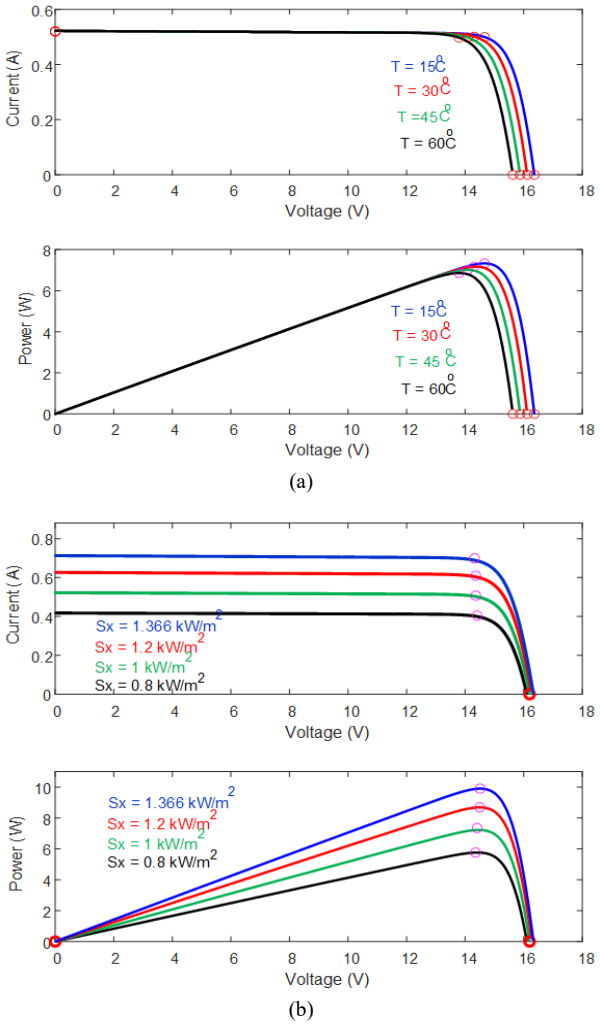

Fig. 10. I-V and P-V characteristics (a) at different temperature level and (b) at different irradiation.

results in a decline in maximum power and a negligible change in the open-circuit voltage of the PV.

B. Dynamic Response of PV with MPPTs at Scenario One

In this scenario, the suggested techniques are examined under the effect of sequence perturbations of irradiance as shown in Fig. 11 and temperature levels. The standard

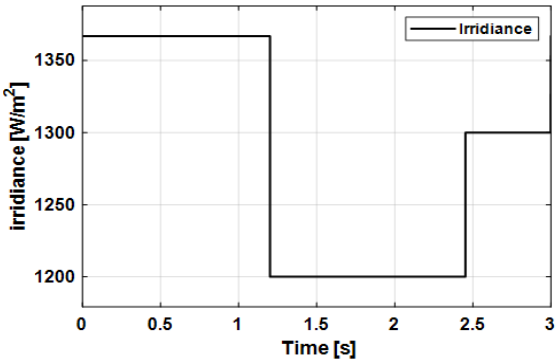

Fig. 11. Change in different levels of irradiance.

irradiance at the beginning was initially 1367 W/m^2 and after 1.2 s a decrement occurred where it reached 1200 W/m^2 and then increased again to 1300 W/m^2 at t= 2.45 s. Therefore, the MPP changed, and output power extracted from the solar PV array also changed due to the varying operating voltage and current.

From Fig. 12, it is noticed that all proposed techniques track the change in power, but the performance is not the same. Table III presents the changes in power and voltage for all variations in irradiance. For P&O, it has lower performance achieved and less power has been extracted from the PV compared to the RCC which delivers higher and smoother power, while the IC provides an even higher power but with some oscillation. In addition, the RCC and IC responses stabilize faster (higher convergence rate) during the moment of radiation changes as shown in Fig. 12 (c). The final finding approves the superiority of RCC in convergence rate as compared to the conventional P&O method.

C. *Dynamic Response of PV with MPPTs at Scenario Two*

In the second scenario, the proposed techniques are examined in the state of 4-rpm spin for a 3U CubeSat. The irradiance level changes on the faces of the satellite while the satellite rotates. The average extracted irradiance of the X-, X+, Y-, and Y+ sides together can be seen in fig. 13. The standard irradiance at the beginning was initially 1000 W/m^2 and after 2.15 s the satellite moved and the Y- side is completely on the standard irradiance of 1367 W/m^2 and then decreased again to 1000 W/m^2 at t= 4.25 sec. A similar phenomenon repeats for the other, X+, Y+ and X- faces. Therefore, the MPP changed, and the output power extracted from the solar PV arrays also changed due to variations in the operating voltage and current can be seen in Fig. 14 (a), (b), and (c).

It can be seen in Fig. 14 (c), that the techniques under comparison track the variations of the power, however, the performance of each tracking technique is not similar. The P&O is extracting less power with more oscillations than the other two techniques. While IC technique is extracting more power as compared to RCC. However, the RCC is smoother and has low oscillations as compared to IC technique. In

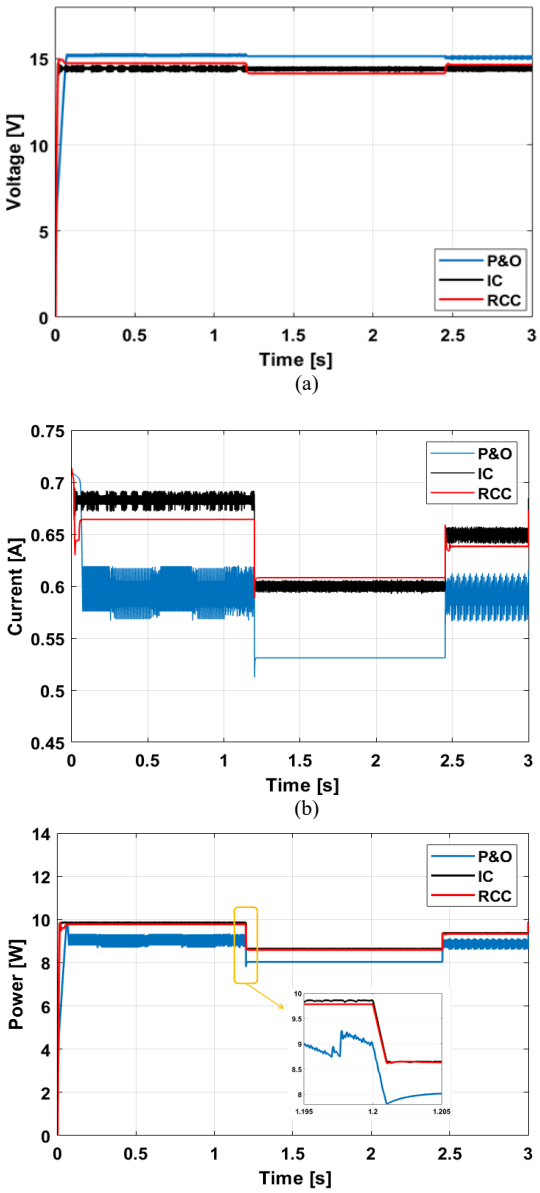

Fig. 12. Comparison of output (a) voltage, (b) current, and (c) power under P&O, IC and RCC.

addition, IC and RCC responses stabilize faster (higher convergence rate) compared to P&O in the moment of radiation changes. The final finding approves the superiority of RCC and IC in convergence rate as compared to the conventional P&O method.

VII. Conclusion

In this paper, some MPPT techniques namely, P&O, IC and RCC are implemented and compared in the case of NanoSat applications under spinning conditions of 4-rpm. Analysis is carried out for two different scenarios. In the first

TABLE III. THE CHANGES IN POWER AND VOLTAGE OF P&O, IC AND RCC IN VARIOUS IRRADIANCE LEVELS

Irradiance level (w/m2)	Switching time (s)	Method	Power (W)	Voltage (V)	Current (A)
1367	At the beginning t= 0 s	P&O	9.1	15.2	0.6
		IC	9.87	14.5	0.683
		RCC	9.78	14.75	0.664
1200	t = 1.2 s	P&O	8.04	15.14	0.53
		IC	8.64	14.4	0.6
		RCC	8.61	14.13	0.608
1300	t= 2.45 s	P&O	8.9	15.1	0.59
		IC	9.38	14.64	0.65
		RCC	9.35	14.44	0.64

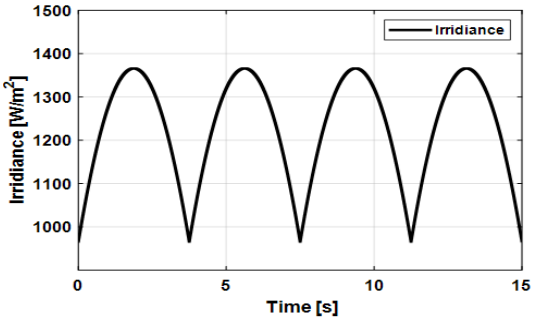

Fig. 13. The average irradiance extracted in t =15 s.

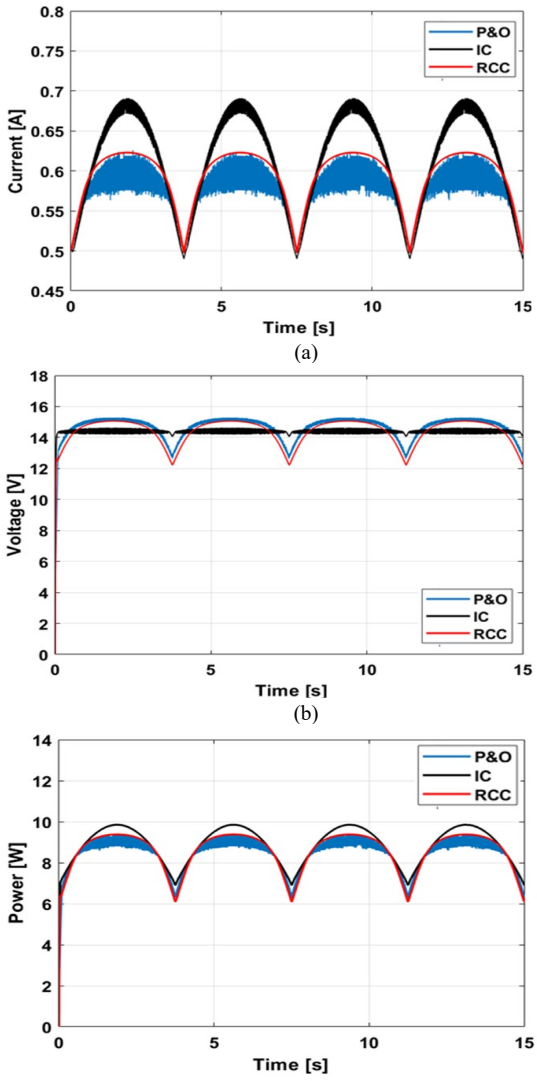

Fig. 14. Comparison of outputs for (a) voltage, (b) current, and (c) power under P&O, IC and RCC at NanoSat spin of 360^0 in 15 s.

scenario the proposed techniques are examined under the effect of sequence perturbations of irradiance and temperature levels. All the techniques track the variations in maximum power but differently. P&O is not very efficient as compared to RCC and IC. RCC which delivers high and smooth power, and the IC which provides high power with some oscillation, both with high convergence rate at solar irradiance change. In the second scenario, the same techniques were examined in 4-rpm spin condition for a 3U CubeSat. The irradiance level changes on the faces of the satellite while the satellite rotates. P&O extracts less power with more oscillations than the other two techniques. While IC technique is extracting more power as compared to RCC. However, RCC is smoother and has low oscillations as compared to IC. In future perspective, the free-orientation and Nadir-orientation conditions are compared in various MPPT scenarios.

ACKNOWLEDGMENT

This work was supported by VILLUM FONDEN under the VILLUM Investigator Grant (no. 25920): Center for Research on Microgrids (CROM); www.crom.et.aau.dk. M. Yaqoob was funded by Balochistan University of Engineering and Technology Khuzdar, Pakistan.

REFERENCES

[1] A. Lashab, M. Yaqoob, Y. Terriche, J.C. Vasquez and J.M. Guerrero, "Space microgrids: New concepts on electric power systems for satellites," IEEE Electrification Magazine, vol. 8, no. 4, pp. 8-19 2020.

[2] M. Yaqoob, M. Nasir, J.C. Vasquez and J.M. Guerrero, "Self-directed Energy Management System for an Islanded Cube Satellite Nanogrid," in 2020 IEEE Aerospace Conference, 2020, pp. 1-7.

[3] S. Sanchez-Sanjuan, J. Gonzalez-Llorente and R. Hurtado-Velasco, "Comparison of the incident solar energy and battery storage in a 3U CubeSat satellite for different orientation scenarios," Journal of Aerospace Technology and Management, vol. 8, pp. 91-102 2016.

[4] A. Ali, A. Massoud, M.O. Hasna, T. Khattab, T. Jabban and M.A. Nema, "Modeling of CubeSat orientation scenario and solar cells for internet of space provision," in 2019 9th International Conference on Recent Advances in Space Technologies (RAST), 2019, pp. 541-546.

[5] L. Peng, Z. Jun, Y. Xiaozhou and C. Luping, "Design and validation of modular MPPT electric power system for multi-U CubeSat," in 2017 3rd IEEE International Conference on Control Science and Systems Engineering (ICCSSE), 2017, pp. 374-377.

[6] H. Abubakr, J.C. Vasquez, K. Mahmoud, M.M. Darwish and J.M. Guerrero, "Comprehensive review on renewable energy sources in Egypt–Current status, grid codes and future vision," IEEE Access 2022.

[7] Y. Xu, G. Wang, C. Zhang, X. Li and Q. Xu, "Research on Integrated MPPT Control and Online Monitoring System of Microsatellite," in 2021 IEEE 5th Advanced Information Technology, Electronic and Automation Control Conference (IAEAC), 2021, pp. 344-348.

[8] M. Lawan, A. Aboushady and K.H. Ahmed, "Photovoltaic MPPT techniques comparative review," in 2020 9th International Conference on Renewable Energy Research and Application (ICRERA), 2020, pp. 344-351.

[9] M.G. Villalva, J.R. Gazoli and E. Ruppert Filho, "Modeling and circuit-based simulation of photovoltaic arrays," in 2009 Brazilian Power Electronics Conference, 2009, pp. 1244-1254.

[10] M. Yaqoob, A. Lashab, J. C. Vasquez, J. M. Guerrero, M. E. Orchard and A. D. Bintoudi, "A Comprehensive Review on Small Satellite Microgrids," in IEEE Transactions on Power Electronics, vol. 37, no. 10, pp. 12741-12762, Oct. 2022, doi: 10.1109/TPEL.2022.3175093.

[11] N. Femia, "Member, IEEE, giovanni petrone, giovanni spagnuolo, member, IEEE, and massimo vitelli "Optimization of perturb and observe maximum power point tracking method,"," IEEE Trans.Power Electron, vol. 20, no. 4, pp. 963-973 2005.

[12] S. Panda, S. Singh, R. Sharma and P.R. Satpathy, "Tracking Comparison of P&O and INC based MPPTs under varying weather conditions," in 2018 2nd International Conference on Data Science and Business Analytics (ICDSBA), 2018, pp. 198-203.

[13] D. Sera, L. Mathe, T. Kerekes, S. V. Spataru and R. Teodorescu, "On the Perturb-and-Observe and Incremental Conductance MPPT Methods for PV Systems," in IEEE Journal of Photovoltaics, vol. 3, no. 3, pp. 1070-1078, July 2013, doi: 10.1109/JPHOTOV.2013.2261118.

[14] S.U. Ramani, S.K. Kollimalla and B. Arundhati, "Comparitive study of P&O and incremental conductance method for PV system," in 2017 International Conference on Circuit, Power and Computing Technologies (ICCPCT), 2017, pp. 1-7.

[15] A. Trivedi, A. Gupta, R.K. Pachauri and Y.K. Chauhan, "Comparison of Perturb & Observe and Ripple correlation control MPPT algorithms for PV array," in 2016 IEEE 1st International Conference on Power Electronics, Intelligent Control and Energy Systems (ICPEICES), 2016, pp. 1-5.

[16] T. Esram, J.W. Kimball, P.T. Krein, P.L. Chapman and P. Midya, "Dynamic maximum power point tracking of photovoltaic arrays using ripple correlation control," IEEE Transactions on power electronics, vol. 21, no. 5, pp. 1282-1291 2006.